FISEVIER

Contents lists available at ScienceDirect

# Journal of Colloid And Interface Science

journal homepage: www.elsevier.com/locate/jcis



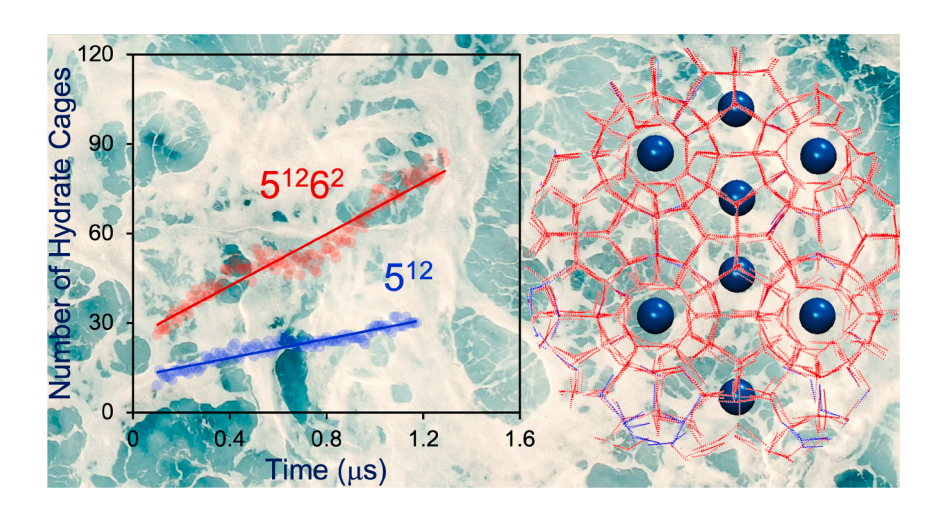


# Microscopic insights on clathrate hydrate growth from non-equilibrium molecular dynamics simulations

Anh Phan a,\*, Michail Stamatakis b, Carolyn A. Koh c, Alberto Striolo b,d,\*

- a School of Chemistry and Chemical Engineering, Faculty of Engineering and Physical Sciences, University of Surrey, Guildford, Surrey GU2 7XH, UK
- <sup>b</sup> Department of Chemical Engineering, University College London, London WC1E 7JE, UK
- <sup>c</sup> Center for Hydrate Research, Chemical & Biological Engineering Department, Colorado School of Mines, Golden, CO 80401, United States
- <sup>d</sup> School of Chemical, Biological and Materials Engineering, University of Oklahoma, Norman, OK 73019, United States

#### GRAPHICAL ABSTRACT



## ARTICLE INFO

Keywords: Methane solubility Binding free energy Adsorption barriers Instantaneous interfaces Interfacial surface area

# $A\ B\ S\ T\ R\ A\ C\ T$

Clathrate hydrates form and grow at interfaces. Understanding the relevant molecular processes is crucial for developing hydrate-based technologies. Many computational studies focus on hydrate growth within the aqueous phase using the 'direct coexistence method', which is limited in its ability to investigate hydrate film growth at hydrocarbon-water interfaces. To overcome this shortcoming, a new simulation setup is presented here, which allows us to study the growth of a methane hydrate nucleus in a system where oil–water, hydrate-water, and hydrate-oil interfaces are all simultaneously present, thereby mimicking experimental setups. Using this setup, hydrate growth is studied here under the influence of two additives, a polyvinylcaprolactam oligomer and sodium dodecyl sulfate, at varying concentrations. Our results confirm that hydrate films grow along the oil–water interface, in general agreement with visual experimental observations; growth, albeit slower, also occurs at the hydrate-water interface, the interface most often interrogated via simulations. The results obtained demonstrate

<sup>\*</sup> Corresponding authors at: School of Chemistry and Chemical Engineering, Faculty of Engineering and Physical Sciences, University of Surrey, Guildford, Surrey GU2 7XH, UK (A. Phan) and School of Chemical, Biological, and Materials Engineering, University of Oklahoma, Norman, OK 73019, United States (A. Striolo).

E-mail addresses: a.phan@surrey.ac.uk (A. Phan), astriolo@ou.edu (A. Striolo).

that the additives present within curved interfaces control the solubility of methane in the aqueous phase, which correlates with hydrate growth rate. Building on our simulation insights, we suggest that by combining data for the potential of mean force profile for methane transport across the oil—water interface and for the average free energy required to perturb a flat interface, it is possible to predict the performance of additives used to control hydrate growth. These insights could be helpful to achieve optimal methane storage in hydrates, one of many applications which are attracting significant fundamental and applied interests.

#### 1. Introduction

The world's changing climate has led to record-breaking temperatures, storms, wildfires, or unprecedented drought across the globe [1]. The Paris Agreement [2] and Kyoto Protocol [3] launched a global effort to mitigate excessive greenhouse gas emissions to reduce impacts and risks of climate change [4]. Various mitigation strategies have been outlined, which entail numerous combinations of low-carbon energy supplies (e.g., solar, wind energy, hydrogen, etc.), reduced energy use, and carbon dioxide (CO<sub>2</sub>) removal [1,4]. Methane (CH<sub>4</sub>), the second most important greenhouse gas, has also attracted attention, for example in the most recent scientific report from the Intergovernmental Panel on Climate Change [5], because CH<sub>4</sub> has 84 times the global warming effect of CO<sub>2</sub> in the first 20 years after emission [5,6]. Indeed, reducing CH<sub>4</sub> emissions can have a fast positive effect on climate [6].

Among various strategies for preventing  $CH_4$  emissions, we focus here on gas hydrates, which are related to a variety of applications, including flow assurance, whose goal is preventing oil and gas pipeline blockage [7-13]. Recent expansions of hydrate applications teeter towards the water-energy-environment nexus, e.g., water desalination [14,15], gas separations [16-19], and storage [20-24]. In particular, the utilization of hydrates for  $CH_4$  capture and storage can be environmentally friendly and cost-effective [20,23]. These potential applications are currently hindered by problems associated with the stochastic nature of hydrate formation, and by the slow kinetics that characterize hydrate growth and dissociation [14]. For instance, increasing the rate of gas hydrate formation is critical in gas storage and separation operations [18,19,24]. Understanding, predicting, and controlling the kinetics of hydrate formation at interfaces [25] is therefore essential for progress. After hydrates nucleate at interfaces, their thickness increases

controlled by mass-transfer [14]. While many experiments focused on hydrate growth at guest-water interfaces [26-29], the common computational approach, known as the 'direct coexistence method' [18,24,30-32], examines hydrate growth within the aqueous phase. We modify here the direct coexistence method to study hydrate growth within a three-phase system. The proposed computational setup allows for the exploration of key phenomena that control the kinetics of hydrate growth at guest-water interfaces.

Implementing non-equilibrium molecular dynamics (MD), we then investigate the growth of a preformed CH<sub>4</sub> hydrate nucleus placed on the surface of a water film immersed in oil (Fig. 1). The hydrocarbon contains CH<sub>4</sub> and *n*-dodecane, and the simulations are conducted at 250 K and 20 MPa. To test the ability of our new setup to assess the effectiveness of hydrate promoters, we quantify the impact of a polyvinylcaprolactam oligomer (identified as CAP throughout the manuscript) and that of sodium dodecyl sulfate (SDS) at various concentrations (see Fig. 1b and c, respectively) on hydrate growth. Although it is known that, thermodynamically, structure *sI* is more stable for methane guest molecules [33], the coexistence of structures *sI* and *sII* hydrates is well documented experimentally, even for pure CH<sub>4</sub> [34,35]. Consistently with these observations, both *sI* and *sII* crystals were used as CH<sub>4</sub> hydrate seeds.

# 2. Simulation methodology

**Hydrate Growth Simulations.** Each simulated system contains one planar sI/sII hydrate crystal shell placed on the surface of the water slab immersed in an oil phase consisted of CH<sub>4</sub> and n-dodecane with a molar ratio of 18.4:10, respectively (see Figs. 1 and S1 in Supporting Information). The initial configuration of a system yields a simulation box

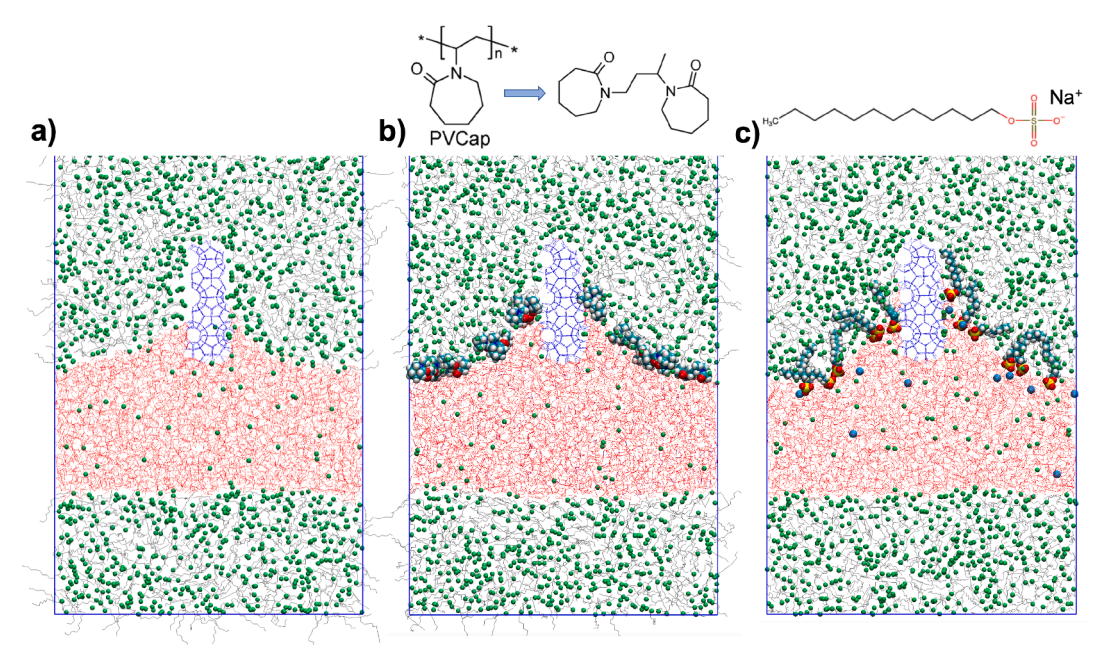


**Fig. 1.** Representative simulation snapshots for the initial configurations for systems composed of one *sI* CH<sub>4</sub> hydrate seed placed on top of a water slab without additives (left), with CAP (middle), and SDS (right) immersed in a hydrocarbon mixture (CH<sub>4</sub> and *n*-dodecane) at 250 K and 20 MPa. Red and blue wireframes symbolize water molecules in the liquid and hydrate phase, respectively, while CH<sub>4</sub> molecules trapped in the hydrate are not shown for clarity. Silver lines represent *n*-dodecane. Green spheres symbolize CH<sub>4</sub>. Red, white, cyan, blue, and yellow spheres represent oxygen, hydrogen, carbon, nitrogen, and sulphur atoms, respectively. (For interpretation of the references to color in this figure legend, the reader is referred to the web version of this article.)

length of 9.731, 3.462, and 18.394 nm in the X-, Y-, and Z-directions, respectively, which comprise a relatively large oil/gas reservoir (~510 nm<sup>3</sup>) and a water film of thickness ~3.9 nm, guaranteeing a low oil/ gas-liquid interfacial curvature and, thus, a negligible Laplace pressure, in contact with the liquid water phase [36]. Equilibrium MD simulations were conducted using the package GROMACS [37]. First, we performed a NVT simulation for 1 ns to relax the initial configuration while the hydrate layer was kept fixed. Subsequently, NPT simulations were conducted at 250 K and 20 MPa implementing a Nose-Hoover thermostat and Berendsen/Parrinello-Rahman barostat [37]. We set to 0.5 ps the time constant for the coupling between the system and the thermostat [37], which removes quickly latent heat from the growing surface [31]. Previous computational studies suggest that the thermostat coupling constant of 0.5 ps is appropriate, achieving excellent agreement against experimental studies for gas hydrate growth [24,33]. Note that based on the phase diagram of water [38], at 250 K and 20 MPa, water is in its supercooled liquid state, which has been used widely for the investigations of clathrate hydrate nucleation and growth mechanisms [33,36,39,40]. We implemented the pressure coupling algorithm only along the *Z*-direction to keep *X* and *Y* dimensions of the simulation box constant. The equations of motion were solved using the leapfrog algorithm with the time step of 1.0 fs [37]. We applied a harmonic restraint force (k = 2000 kJ/mol·nm) on water and CH<sub>4</sub> molecules in the hydrate shell to tether them to their initial positions while other molecules in the system were allowed to move in the simulations [37]. During the crystal hydrate growth simulation, the water molecules were allowed to move freely; however, the center of mass of the water slab was tethered by a harmonic spring of elastic constant 20,000 kJ/mol.nm [37] so that the water slab is kept underneath the constrained hydrate shell. This approach enables the observation of lateral hydrate growth at the interface. This set up mimics the experimental setting [41], in which hydrate formation is induced at the top of a sessile water drop by contact with a hydrate seed attached at the tip of a fixed capillary tube. The curved oil-water interface near the hydrate seed (see Fig. 1), which is due to the strong water wettability of the hydrate surfaces [42], appear similar to visual analysis of experimental images [41]. To achieve statistically reliable numerical results from our calculations, we conducted each simulation for 1200–1600 ns, equivalent to ~480–640 CPU hours. Two independent hydrate growth simulation runs with different initial velocities were performed for each system to assess uncertainty. To ensure the generalizability of the conclusions, we repeated the simulations for two different hydrate structures. The total computational cost for all simulation systems considered in this study reaches tens of thousands of core hours (~12,000 CPU hours).

Interfacial Properties. To evaluate CH<sub>4</sub> solubility, fluid–fluid interfacial tensions, and interfacial surface area, we conducted  $\sim 200$  ns NPT simulations for each system composed of the oil–water interface at 250 K and 20 MPa. The oil–water interface model was generated by combining aqueous and oil phases into  $5.804 \times 5.804 \times \sim 19.540 \, (\text{nm}^3)$  simulation boxes, as shown in Fig. S2 in Supporting Information. To confirm the simulations reached equilibrium, we analyzed the convergence of system energy as well as water, CH<sub>4</sub>, and *n*-doecane density profiles along the direction perpendicular to the oil–water interfaces. We implemented similar approaches to estimate fluid–fluid interfacial tensions for a variety of systems [42–46].

To study the effect of CAP/SDS additives on hydrate growth, we placed a layer of these additives on the surface of the water slab at various concentrations in the range of 0.03–0.36 molecules/nm². Note that surfactants accumulate at interfaces even at very low bulk concentrations [47]. Because our aim is to quantity the effect of surfactants on hydrate growth and other interfacial properties, no CAP/SDS are present in the bulk solutions simulated here. The total number of atoms in the systems ranged from 34,240 to 34,816. Error bars were obtained from three independent simulation runs for each system.

**Force Fields.** Water was represented by the TIP4P/Ice model [48], which has been successful in simulating hydrate nucleation and growth

[24,33]. CH<sub>4</sub> and *n*-dodecane were represented by the united-atom version of the TraPPE-UA force field [49], which accurately characterizes the vapor-liquid coexistence curves and critical properties of linear alkanes from methane to dodecane. CAP and SDS additives were modelled implementing the General Amber Force Field (GAFF) [50,51], often employed to study organic and pharmaceutical molecules containing H, C, N, O, S, P, and halogens [50]. Na<sup>+</sup> ions were modeled as charged Lennard-Jones (LJ) spheres by using the parameters suggested by Dang [52], which is compatible with various water models [25,53]. All non-bonded interactions were described using 12-6 Lennard-Jones (LJ) potentials with the cutoff distance of 1.4 nm. The electrostatic interactions were modeled by the Coulombic potential with long-range corrections treated using the particle-particle particle-mesh (PPPM) approach [54]. We utilized the Lorentz-Berthelot combining rules to quantify unlike LJ interactions [55]. Several computational studies suggest that combining GAFF for modelling cyclic and organic molecules, TIP4P/Ice model for water, and TraPPE-UA for linear alkanes yields excellent agreement against experimental studies [12,13,24,56].

## 3. Results and discussion

Hydrate Growth Kinetics. In Fig. 2a, we present simulation snapshots that illustrate the growth of one *sI* CH<sub>4</sub> hydrate seed deposited on the water surface at 250 K and 20 MPa, in the absence of additives. As the MD simulations progress, CH<sub>4</sub> molecules are dissolved in supercooled liquid water, leading to the growth of the hydrate shell along the oil–water interface, in qualitative agreement with experiments, even though growth also happens, more slowly, at the hydrate-water interface [26,27,41]. Because the total number of CH<sub>4</sub> molecules was maintained constant throughout the simulations, the more CH<sub>4</sub> molecules are present in supercooled liquid water, the further the CH<sub>4</sub> molar fraction in the oil phase is reduced, qualitatively consistent with the experimental observations reported by Hassanpouryouzband et al. [57]. We observe similar growth patterns for *sI* hydrates in the presence of two and twelve CAP/SDS molecules, corresponding to 0.06 and 0.36 molecules of additives per nm<sup>2</sup> (see Fig. S3 in Supporting Information).

To quantify hydrate structural growth, the cage type and cage occupancy were evaluated using the topological-algorithm-assisted cage identification [58]. The results were averaged over  $\sim 10$  ns time windows to achieve acceptable data visualization. In Fig. 2b-d, we report the number of various types of hydrate cages, e.g., 12-hedron (5<sup>12</sup>, blue), 14-hedron ( $5^{12}6^2$ , red), 16-hedron ( $5^{12}6^4$ , green), as a function of simulation time for systems composed of sI/sII hydrate without additives (b), in the presence of CAP (c) or SDS (d) at various concentrations. The number of hydrate cages grows linearly for all systems. Fitting the results with a linear curve, we extract the cage growth rates: the growth rate of sI  $5^{12}6^2$  cages (~43–51 cages/ns as obtained by fitting the simulation results) is nearly three times that of the sI  $5^{12}$ -cage one ( $\sim$ 15 cages/ns), whereas the growth rate of sII  $5^{12}6^4$  cages (~2–3 cages/ns) is ~two times slower than the sII 5<sup>12</sup>-cage one (~5–9 cages/ns). These observations are consistent with the fact that one sI 5<sup>12</sup> cage grows with three sI 5<sup>12</sup>6<sup>2</sup> cages (the ratio of 5<sup>12</sup> to 5<sup>12</sup>6<sup>2</sup> cages of 1:3), while one sII 5<sup>12</sup>6<sup>4</sup> cage grows with two sII 5<sup>12</sup> cages in an ideal condition (the ratio of  $5^{12}$  to  $5^{12}6^4$  cages of 2:1) [59]. Our results also show that the growth rate of sI 5<sup>12</sup> cages (~15 cages/ns) is much higher than that of the sII cages ( $\sim$ 5–9 cages/ns), reflecting the fact that the sI is the thermodynamically stable phase of CH<sub>4</sub> hydrate at  $T \le 293$  K and  $P \le 100$  MPa [34].

From the results shown in Fig. 2c, we observe negligible differences in the growth rate of sI hydrate in the presence of two/twelve CAP compared to the results obtained for the system without chemical additives (~43  $5^{12}6^2$ -cages/ns) (Fig. 2b). Contrarily, the growth rate of sII hydrate in the presence of two CAP (~9  $5^{12}$ -cages/ns) is greater than that obtained without additives (~5  $5^{12}$ -cages/ns). Examining further the simulation snapshots of the sI hydrate growth with two CAP present, we notice that after ~0.5  $\mu$ s, one CAP adsorbed on the formed hydrate cages, while the other moved away, remaining at the water–oil

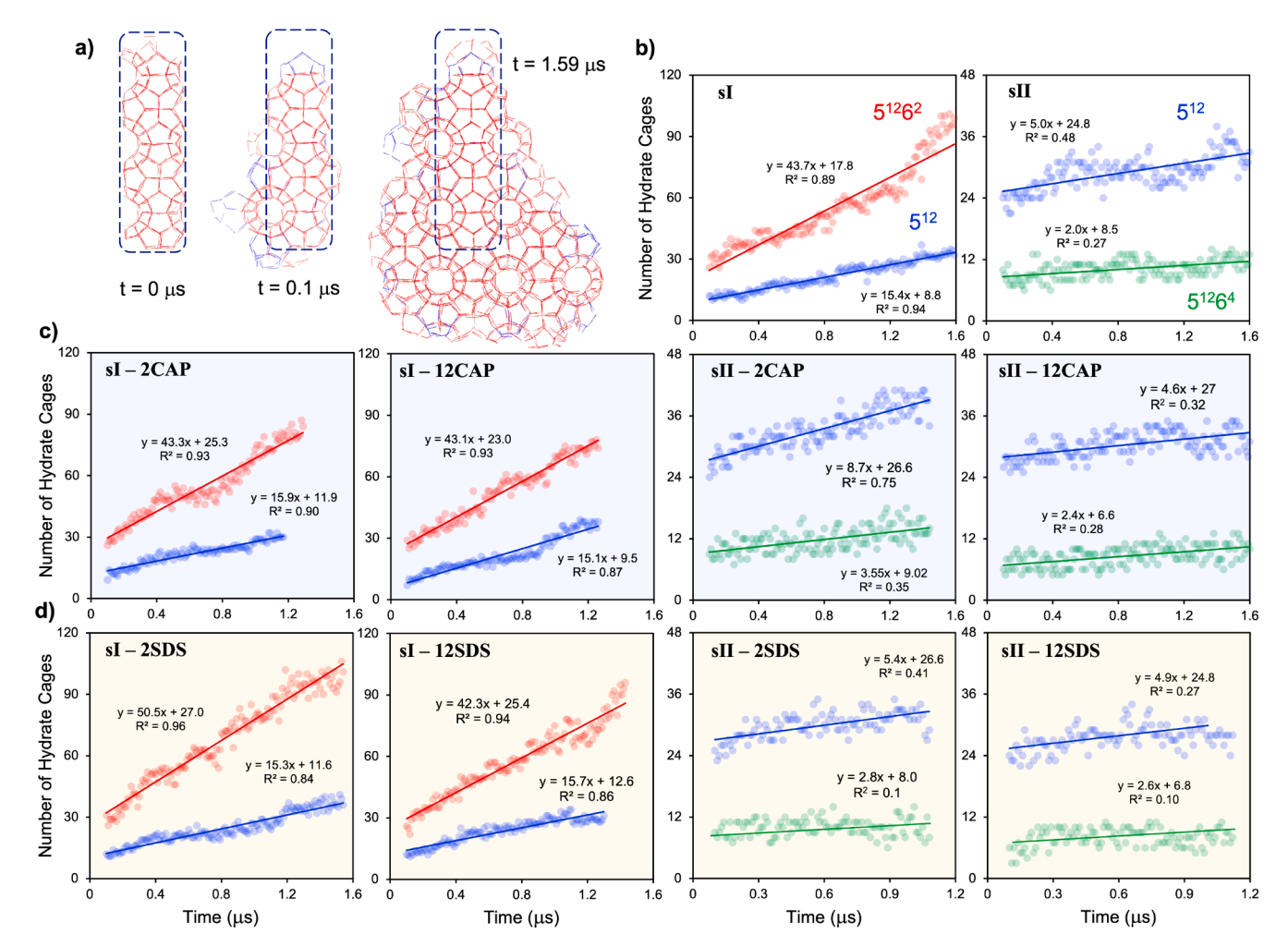


**Fig. 2.** (a) Snapshots of a simulated sI CH<sub>4</sub> hydrate seed growing during our simulations. The seed had been placed on the surface of the water slab at 250 K and 20 MPa. The results are shown at increasing simulation times, e.g., 0, 0.1, and 1.59 μs. Additives are not present in these simulations. Evolution of number of various types of hydrate cages, e.g., 12-hedron ( $5^{12}$ , blue), 14-hedron ( $5^{12}6^2$ , red), and 16-hedron ( $5^{12}6^4$ , green), as a function of time for systems composed of the sI/sII CH<sub>4</sub> hydrate without additives (b), in the presence of CAP (c), or SDS (d) at various concentrations. (For interpretation of the references to color in this figure legend, the reader is referred to the web version of this article.)

interface. This possibly causes the decrease in the sI hydrate growth rate observed after 0.5  $\mu$ s. Of note, within the first 0.5  $\mu$ s simulation time, we obtain a higher growth rate for the sI hydrate in the presence of two CAP (~59  $5^{12}6^2$ -cages/ns), which is consistent with the results obtained for the sII hydrate.

The results just described are unexpected, as infrared spectroscopy data [60] indicate that CAP behaves similarly, in terms of its interaction with water, to the commercial PVCAP, a known kinetic hydrate inhibitor (KHI). PVCAP is thought to bind to the hydrate-water interface and delay hydrate growth [61,62]. Note that KHIs are most effective at moderate subcooling conditions and when no liquid hydrocarbon phase is present [63,64]. The subcooling employed in this study is  $\sim$ 40 °C [65], which is much larger than the effective subcooling limits for PVCAP of 18 °C [66]. Nevertheless, when CAP additives are immersed within the aqueous phase and interact with the hydrate phase, we observe that they can hinder hydrate growth (see Fig. S4 in Supporting Information), consistent with other studies [61,62].

The results presented in Fig. 2d show the higher growth rate of sI/sII hydrates in the presence of two SDS molecules (yielding 0.06 molecules/nm²) compared to results obtained without additives. One experimental study [41] reported that SDS at low concentrations enhances the lateral CH<sub>4</sub> growth rate at CH<sub>4</sub>-water interfaces at 0 °C and 4 MPa (1.55 vs 1.18 mm/s obtained without SDS). At such conditions, literature experiments and our computational results agree that SDS is an effective promoter for

CH<sub>4</sub> hydrate growth at hydrocarbon-water interfaces. On the other hand, twelve SDS (0.36 molecules/nm<sup>2</sup>) at the interface show insignificant impact on the growth rate compared to when no additive is present. These unexpected results are qualitatively consistent with Sangwai et al. [67], who reported that excessive SDS inhibited CH<sub>4</sub> hydrate growth oil-in-water dispersion systems at 8 MPa and 275.15 K. Comparing the results shown in Fig. 2c with those reported in Fig. 2d, we observe that CAP promotes the growth rate of *sI/sII* hydrates more strongly than SDS at low concentrations; however, at high concentrations, neither CAP nor SDS accelerate the hydrate growth rate. These results are summarized in Fig. 3.

Relation between Hydrate Growth Kinetics and CH<sub>4</sub> Solubility. Our simulation results (see procedure in Supporting Information) show that the average growth rate of sI hydrate is  $\sim$ 9.0 mm/s while the sII growth rate is  $\sim$ 0.5 mm/s in the absence of additives (see Fig. 3). These data are qualitatively consistent with the ones obtained from extrapolating the experimental data of the hydrate growth rate linearly correlated with the subcooling ( $\sim$ 12.6 mm/s) [41] at similar subcooling conditions ( $\sim$ 40 °C). However, because these experimental data were obtained at CH<sub>4</sub>-water interfaces when the hydrate seed was placed on top of the water droplet immersed in bulk CH<sub>4</sub> [41], further experimental studies should be conducted at conditions representative of our simulation set up (i.e., with the oil–water interfaces) to verify the agreement between experiments and simulations.

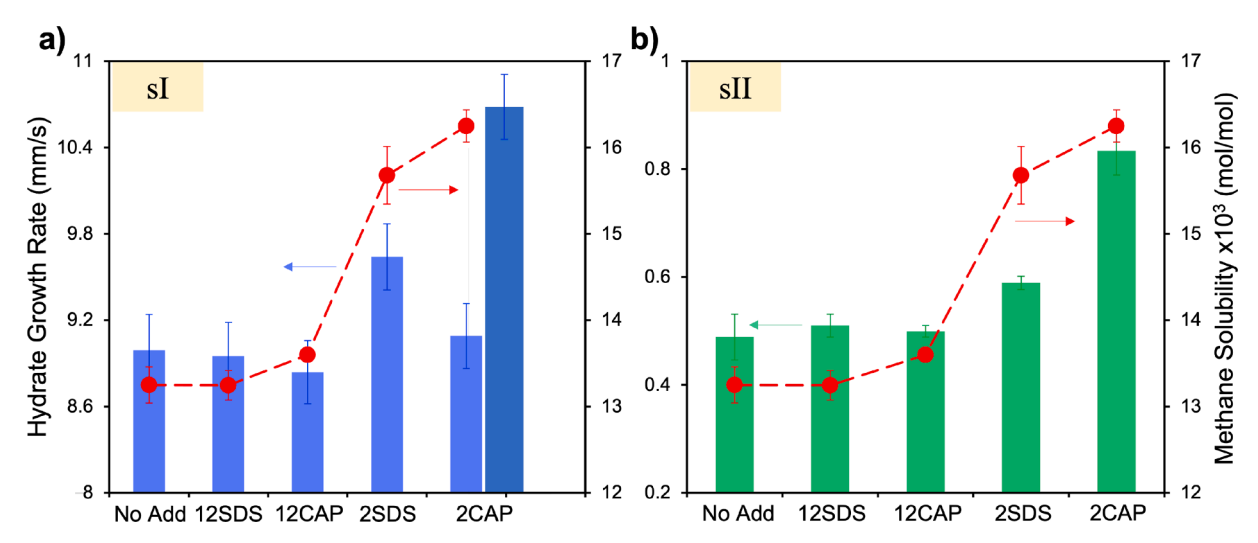


**Fig. 3.** Crystal growth rate (bars) of *sI* (a) and *sII* (b) CH<sub>4</sub> hydrates at the oil–water interface at 250 K and 20 MPa associated with the relevant methane solubility (red filled circles) obtained for systems without chemical additives and with CAP/SDS at various concentrations. Dashed lines are guides to the eye. Results obtained for the '2CAP' system in panel (a) are obtained by fitting the simulation results within two different time intervals. Please refer to the text for details. Error bars were obtained from two independent simulation runs for each system. (For interpretation of the references to color in this figure legend, the reader is referred to the web version of this article.)

In Fig. 3a, our results show that CAP and SDS impact the growth rate in the following order: no additives  $\approx$  twelve SDS  $\approx$  twelve CAP < two SDS < two CAP molecules (dark blue, see Fig. 3a). (For a discussion on results obtained at low CAP concentration, refer to SI). Analogous trends are observed for sII hydrates (see Fig. 3b). Our simulation results show that the difference in the hydrate growth rate between the systems with two SDS and without SDS molecules is  $\sim\!0.65$  mm/s, which is qualitatively comparable to the experimental data ( $\sim\!0.37$  mm/s) obtained at CH4-water interfaces in the presence of low SDS concentrations at 0  $^{\circ}$ C and 4 MPa [41].

Several studies [68,69] have attributed enhanced hydrate growth to the formation of micelles, while many others strongly object, claiming that micelles do not form under typical hydrate-forming conditions [70,71]. Our results show that the promoting effect due to SDS is not a result of micelles. Other possible mechanisms are enhanced mass transport rate and enhanced CH<sub>4</sub> solubility [9,72]. We first test the correlation between hydrate growth rate and CH<sub>4</sub> solubility by conducting complementary simulations for systems composed of the oilwater interface without hydrates (see Fig. S2 in Supporting Information). Our results reveal that CH4 solubility increases in the order: no additives  $\approx$  twelve SDS  $\approx$  twelve CAP < two SDS < two CAP molecules (see Fig. S5 in Supporting Information), which is directly correlated with hydrate growth rate (Fig. 3). In Fig. S5, we also observe that the CH<sub>4</sub> solubility in the presence of one CAP is comparable to those obtained when no additives are used, or when twelve CAP are present, explaining why the sI hydrate growth rate decreases after one CAP adsorbs on the growing hydrate (Fig. 3a, light blue).

Recently, Lin et al. [73] studied the properties of  $CH_4$ /water two-phase systems with SDS to understand promoting effects on  $CH_4$  hydrate nucleation and growth.  $CH_4$  solubility remained nearly unchanged upon loading SDS [73]. However, it should be noted that Lin et al. [73] used SDS at higher concentrations (0.52–2.08 molecules/nm²) than those considered here. Note that our simulation results show comparable  $CH_4$  solubility achieved for both systems without SDS and with twelve SDS (0.36 molecules/nm²), which is qualitatively consistent with the results reported by Lin et al. [73].

One fundamental question arises from Fig. 3: how can CAP and SDS significantly alter the  $CH_4$  solubility, controlling the  $CH_4$  hydrate growth rate at the oil—water interface, if they are adsorbed only on one interface of the system shown in Fig. 1? It has been proposed [9,72] that surfactants lower the interfacial tension and adhesion energy, reducing

barriers to mass transport and therefore increasing  $CH_4$  solubility. Our simulations show that the interfacial tension decreases with increasing CAP/SDS density at the oil–water interface; this is qualitatively consistent with literature [45,73,74] (see Fig. S6 in Supporting Information), but not consistent with the trends for the hydrate growth rate shown in Fig. 3.

Barriers to Adsorption. We conducted thermodynamic calculations to unravel the interplay of CH<sub>4</sub>, CAP/SDS at different concentrations, oil solvents, and water with respect to CH<sub>4</sub> solubility. In Fig. 4, we present potential of mean force (PMF) profiles (obtained by umbrella sampling simulations [37] analyzed with the weighted histogram method [76]) experienced by one CH<sub>4</sub> molecule as it approaches perpendicularly the oil-water interface from the oil phase. The results are shown as functions of the distance l between the center of one CH4 molecule and the interface. The PMF profiles depend on the type and concentration of additives. Specifically, in the absence of additives (blue) or in the presence of two CAP/SDS molecules (green), the PMF profiles show an effective attraction between CH4 and the interface, a result of the attractive dispersion interactions between CH<sub>4</sub> and the interfacial water molecules [73,77,78], followed by a repulsive barrier at shorter distances towards water, possibly due to the disrupted hydrogen-bond network of water molecules near CH<sub>4</sub> [79]. On the other hand, the PMFs obtained in the presence of twelve CAP/SDS molecules (red) show one repulsive barrier at intermediate l, a minimum, and one much larger repulsive barrier near the interface, probably due to the steric hindrance caused by the higher additive concentration. Our simulation results are qualitatively consistent with those reported by Lin et al. [73] who showed an increased relative free energy barrier with the density of SDS at the interface. By integrating the PMF profiles within the effective attraction part for systems without and with two CAP/SDS, we obtain the effective binding free energy:  $\Delta G_{bind} = \left(-k_BT ln \int^{bound} e^{-\varphi_i/k_BT} dl\right)$ 

 $\left(-k_BTln\int^{unbound}e^{-\varphi_i/k_BT}dl\right)$  where  $\varphi_i$  is the PMF value associated with the  $i^{th}$  bin along the distance l [25]. The results show that  $\Delta G_{bind}$  increases in the following order: no additives (21.8  $\times$  10 $^2$  J/mol)  $\approx$  two SDS (21.2  $\times$  10 $^2$  J/mol) < two CAP (24.2  $\times$  10 $^2$  J/mol). It can also be seen that the PMF height barriers for CH<sub>4</sub> transport in the systems with two CAP/SDS molecules (6.2 kJ/mol) are smaller than the one obtained for the system without chemical additives ( $\sim$ 7.2 kJ/mol), explaining why CH<sub>4</sub> moves across the interface more easily, leading to faster hydrate growth rate, in the order: no additives < two SDS < two CAP.

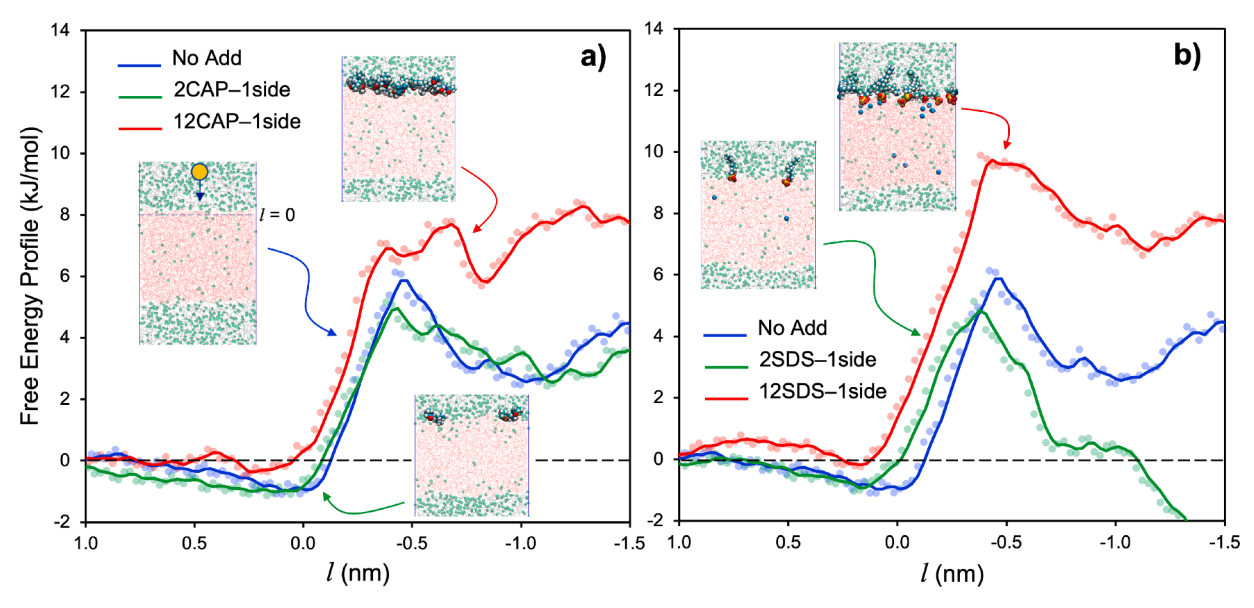


**Fig. 4.** Potential of mean force (PMF) profiles along the *Z* direction (perpendicular to the oil–water interface) experienced by one CH<sub>4</sub> molecule in the oil phase moving toward the aqueous phase. The results were obtained for systems without additives (blue) and with CAP (a) or SDS (b) at various concentrations. The insets show representative simulation snapshots for the configurations for the systems in the absence of additives and with the presence of CAP/SDS at 250 K and 20 MPa. The color scheme is the same as that of Fig. 1. The reference (l = 0) corresponds to the position of interface estimated using the procedure proposed by Willard and Chandler [75]. (For interpretation of the references to color in this figure legend, the reader is referred to the web version of this article.)

Complementing the results just discussed, the PMF height barriers for CH<sub>4</sub> transport  $\Delta G_{barrier}$  increase in the order: no additives (7.2 kJ/mol) < twelve CAP (8.3 kJ/mol) < twelve SDS (10.1 kJ/mol). This is likely due to the enhanced alignment of water molecules at the interface induced by the interfacial electric field due to the adsorption of ionic surfactants, e.g., SDS, which impede CH<sub>4</sub> migration to the water phase [80,81]. The CH<sub>4</sub> solubility obtained for these systems follows a different trend: no additives  $\approx$  twelve SDS  $\approx$  twelve CAP. This suggests that, although PMF profiles might be important for explaining the CH<sub>4</sub> solubility at low CAP/SDS concentrations, they are not sufficient to explain our results.

Willard-Chandler Surface. Ansari et al. [82] proposed that the local interfacial curvature affects the diffusion mechanism of gas molecules across interfaces, suggesting that the large available free area on the crest region of the interface accelerates gas diffusion into the liquid phase. Because of the significant contribution of the interfacial surface area to CH<sub>4</sub> transport across the oil–water interface, we computed the interfacial surface area of all systems using the procedure proposed by Willard and Chandler (WC) [75]. To implement this approach, we adopted the suggested coarse-graining length of 0.24 nm and a 50% water bulk density criterion [75,83]. In Fig. 5a, we present simulation snapshots for the configurations for the systems in the presence of twelve CAP (left) and twelve SDS (right) molecules at 250 K and 20 MPa with two WC interfaces.

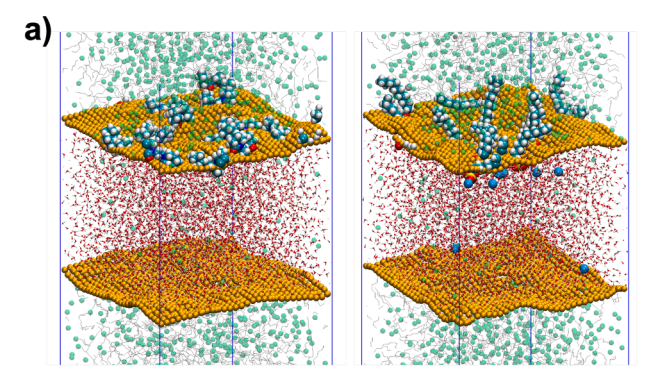
The ensemble average values of the interfacial area are obtained by averaging individual areas of an instantaneous WC interface for each system. The normalized change in the interface area,  $\Delta A$ , is measured relative to a flat surface having the same *X-Y* dimension as  $\Delta A = \langle A(WC) - A \rangle$  [84], where A(WC) is the area of the WC surface, and A is the area of the flat surface (33.69 nm²).  $\Delta G_{def}$  is defined as the average free energy required to perturb a flat interface to an interface with the capillary wave structure with the following expression [85]  $\Delta G_{def} = \gamma \times \Delta A = \gamma \times \langle A(WC) - A \rangle$ , where  $\gamma$  is the interfacial tension. In Fig. 5b, we report  $\Delta G_{def}$  (blue columns) associated with CH<sub>4</sub> solubility (red dotted lines) for systems without additives and with CAP/SDS.  $\Delta G_{def}$  values increase in the order: no additives < two CAP  $\approx$  two SDS < twelve CAP < twelve SDS, suggesting that greater  $\Delta G_{def}$  (or larger A(WC)) are achieved upon loading CAP/SDS. Our results also show that SDS can perturb a flat interface more strongly than CAP at high concentrations. Although

it might be expected that greater  $\Delta G_{def}$  helps enhancing CH<sub>4</sub> transport [82], yielding an increased CH<sub>4</sub> solubility, we observe no correlations between  $\Delta G_{def}$  and CH<sub>4</sub> solubility for the systems considered here (see Fig. 5b). Remarkably, we notice that the values of the PMF barriers for CH<sub>4</sub> transport increase in the order: no additives < twelve CAP < twelve SDS, corresponding to the increased order of  $\Delta G_{def}$  for these systems. This indicates that although loading CAP/SDS could cause steric hindrance, it could increase the interfacial surface area and thus accelerate CH<sub>4</sub> transport into the aqueous phase, which could possibly help explain why the CH<sub>4</sub> solubility and hydrate growth rate for the systems with twelve CAP/SDS are comparable to the ones obtained without additives.

Fitting  $\Delta G_{def}$ , effective binding free energy  $\Delta G_{bind}$ , and barriers to adsorption  $\Delta G_{barrier}$  obtained for all systems considered to the multilinear regression model  $f(\Delta G) = a \times \Delta G_{def} + b \times \Delta G_{bind} + c \times \Delta G_{barrier}$ , we observe a direct relationship between  $f(\Delta G)$  and CH<sub>4</sub> solubility with a=1.05, b=5.06, and c=-3.09 (see Fig. S7 in Supporting Information). These results suggest that PMF profiles for CH<sub>4</sub> transport ( $\Delta G_{bind}$  and  $\Delta G_{barrier}$ ) and average free energy  $\Delta G_{def}$  required to perturb a flat interface provide comprehensive understanding of the gas migration across the oil–water interface, and hence, indirectly, can quantify and potentially predict the kinetics of hydrate growth. More extensive studies, conducted for a variety of chemical additives at different concentrations, should be conducted, perhaps guided by a design of experiment approach, to assess whether this correlation is general.

## 4. Conclusions

In conclusion, we propose a new non-equilibrium MD simulation setup that has allowed us to study hydrate growth within a three-phase model system that closely mimics experimental studies [26,28,29,41]. This computational approach overcomes the limitation of 'direct coexistence method' commonly used for the study of hydrate growth within the aqueous phase [18,24,30-32]. The simulation results show the growth of hydrate seeds along the oil–water interface, qualitatively consistent with experimental studies [41], notwithstanding the crystal also grows, more slowly, at the hydrate-water interface. We employed the new non-equilibrium MD simulation setup to delve into the impact of two chemical additives, a poly vinyl caprolactam oligomer and sodium dodecyl sulfate. Non-monotonic effects between the additive



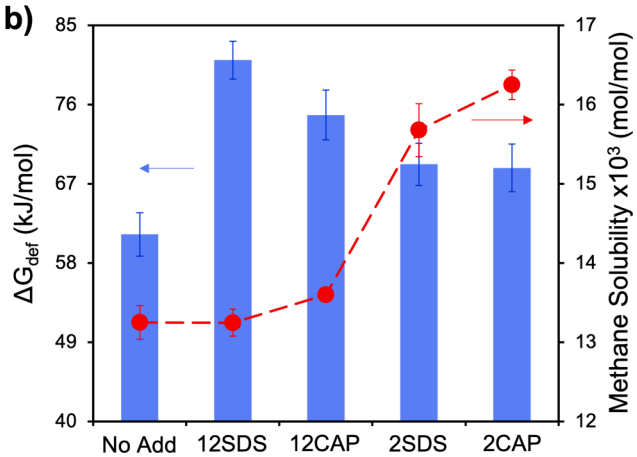


**Fig. 5.** (a) Simulation snapshots for the configurations for the systems in the presence of twelve CAP/SDS molecules at the top oil–water interface at 250 K and 20 MPa. The color scheme is the same as that of **Fig. 1**. Two Willard-Chandler water interfaces are shown in dark yellow. (b) Average free energy  $\Delta G_{def}$  (bars) required to perturb a flat interface to an interface with the capillary wave structure associated with relevant CH<sub>4</sub> solubility (red filled circles) obtained for systems without additives and with CAP/ SDS at various concentrations at the interface. (For interpretation of the references to color in this figure legend, the reader is referred to the web version of this article.)

concentration and hydrate growth rate were observed, perhaps unexpected, yet in agreement with some experimental observations [41,67]. A direct correlation was revealed between hydrate growth rate and methane solubility in the aqueous phase. Furthermore, careful analysis of the simulation results unveiled some of the key factors which might determine the performance of chemical additives used to govern hydrate growth kinetics. These include the potential mean force profile for methane transport across the oil–water interface and the average free energy required to perturb a flat interface. Multi-variate linear regression of these quantities is found to strongly correlate with methane solubility and hydrate growth rate. These new atomistic insights not only complement experimental observations [41,67], but could also be exploited for bottom-up design of new chemical additives towards maximizing the efficiency of greenhouse gas storage in hydrates in future studies.

# ${\it CRediT\ authorship\ contribution\ statement}$

Anh Phan: Conceptualization, Methodology, Investigation, Visualization, Writing – original draft. Michail Stamatakis: Funding acquisition, Writing – review & editing. Carolyn A. Koh: Funding acquisition, Writing – review & editing. Alberto Striolo: Conceptualization, Funding acquisition, Writing – review & editing.

#### **Declaration of Competing Interest**

The authors declare that they have no known competing financial interests or personal relationships that could have appeared to influence the work reported in this paper.

### Data availability

Data will be made available on request.

### Acknowledgments

Financial support was generously provided, in part, by the UK EPSRC, under grant number EP/T004282/1 (AS, MS), and by the US National Science Foundation, under grant number CBET 2015201 (CAK). Generous allocations of computing time were provided by ARCHER2, the UK National Supercomputing Service (<a href="http://www.archer2.ac.uk">http://www.archer2.ac.uk</a>).

# Appendix A. Supplementary material

Supplementary data to this article can be found online at https://doi.org/10.1016/j.jcis.2023.06.032.

#### References

- [1] The other important greenhouse gas, C&EN Global Enterprise 99 (2021) 28-33.
- [2] U.N.F.C.o.C. Change, Adoption of the Paris Agreement, in: 21st Conference of the Parties, Paris, 2015.
- [3] U.N.F.C.O.C. Change, Kyoto Protocol Reference Manual on Accounting of Emissions and Assigned Amount, 2008.
- [4] A. Hassanpouryouzband, E. Joonaki, K. Edlmann, R.S. Haszeldine, Offshore geological storage of hydrogen: is this our best option to achieve net-zero? ACS Energy Lett. 6 (2021) 2181–2186.
- [5] I.P.o.C. Change, AR6 Synthesis Report: Climate Change 2022, 2022.
- [6] R.B. Jackson, M. Saunois, P. Bousquet, J.G. Canadell, B. Poulter, A.R. Stavert, P. Bergamaschi, Y. Niwa, A. Segers, A. Tsuruta, Increasing anthropogenic methane emissions arise equally from agricultural and fossil fuel sources, Environ. Res. Lett. 15 (2020), 071002.
- [7] A. Striolo, Clathrate hydrates: recent advances on CH4 and CO2 hydrates, and possible new frontiers, Mol. Phys. (2019).
- [8] A. Striolo, A. Phan, M.R. Walsh, Molecular properties of interfaces relevant for clathrate hydrate agglomeration, Curr. Opin. Chem. Eng. 25 (2019) 57–66.
- [9] L.E. Zerpa, J.L. Salager, C.A. Koh, E.D. Sloan, A.K. Sum, Surface chemistry and gas hydrates in flow assurance, Ind. Eng. Chem. Res. 50 (2011) 188–197.
- [10] Z.M. Aman, C.A. Koh, Interfacial phenomena in gas hydrate systems, Chem. Soc. Rev. 45 (2016) 1678–1690.
- [11] P.M. Naullage, A.A. Bertolazzo, V. Molinero, How do surfactants control the agglomeration of clathrate hydrates? Acs Central Sci. 5 (2019) 428–439.
- [12] T. Bui, A. Phan, D. Monteiro, Q. Lan, M. Ceglio, E. Acosta, P. Krishnamurthy, A. Striolo, Evidence of structure-performance relation for surfactants used as antiagglomerants for hydrate management, Langmuir 33 (2017) 2263–2274.
- [13] A. Phan, M. Stamatakis, C.A. Koh, A. Striolo, Correlating antiagglomerant performance with gas hydrate cohesion, Acs Appl. Mater. Inter. 13 (2021) 40002–40012.
- [14] A. Hassanpouryouzband, E. Joonaki, M.V. Farahani, S. Takeya, C. Ruppel, J. H. Yang, N.J. English, J.M. Schicks, K. Edlmann, H. Mehrabian, Z.M. Aman, B. Tohidi, Gas hydrates in sustainable chemistry, Chem. Soc. Rev. 49 (2020) 5225–5309.
- [15] P. Babu, A. Nambiar, T.B. He, I.A. Karimi, J.D. Lee, P. Englezos, P. Linga, A review of clathrate hydrate based desalination to strengthen energy-water nexus, ACS Sustain. Chem. Eng. 6 (2018) 8093–8107.
- [16] N.I. Papadimitriou, I.N. Tsimpanogiannis, I.G. Economou, A.K. Stubos, Monte Carlo simulations of the separation of a binary gas mixture (CH4 + CO2) using hydrates, PCCP 20 (2018) 28026–28038.
- [17] R. Kumar, P. Englezos, I. Moudrakovski, J.A. Ripmeester, Structure and composition of CO2/H-2 and CO2/H-2/C3H8 hydrate in relation to simultaneous CO2 capture and H-2 production. AIChE J 55 (2009) 1584–1594.
- [18] J. Pang, Y. Liang, Y. Masuda, S. Takeya, Structural transition of the methaneethane mixture hydrate in a hydrate/water/hydrocarbon three-phase coexistence system: effect of gas concentration, ACS Sustain. Chem. Eng. 8 (2020) 16924–16937.
- [19] N.N. Nguyen, C.V. Nguyen, T.A.H. Nguyen, A.V. Nguyen, Surface science in the research and development of hydrate-based sustainable technologies, ACS Sustain. Chem. Eng. 10 (2022) 4041–4058.
- [20] M. Khurana, H.P. Veluswamy, N. Daraboina, P. Linga, Thermodynamic and kinetic modelling of mixed CH4-THF hydrate for methane storage application, Chem. Eng. J. 370 (2019) 760–771.

- [21] D.Y. Koh, H. Kang, J. Jeon, Y.H. Ahn, Y. Park, H. Kim, H. Lee, Tuning cage dimension in clathrate hydrates for hydrogen multiple occupancy, J. Phys. Chem. C 118 (2014) 3324–3330.
- [22] T. Sugahara, J.C. Haag, P.S.R. Prasad, A.A. Warntjes, E.D. Sloan, A.K. Sum, C. A. Koh, Increasing hydrogen storage capacity using tetrahydrofuran, J. Am. Chem. Soc. 131 (2009) 14616-+.
- [23] H.P. Veluswamy, A.J.H. Wong, P. Babu, R. Kumar, S. Kulprathipanja, P. Rangsunvigit, P. Linga, Rapid methane hydrate formation to develop a cost effective large scale energy storage system, Chem. Eng. J. 290 (2016) 161–173.
- [24] A. Phan, H. Schlösser, A. Striolo, Molecular mechanisms by which tetrahydrofuran affects CO2 hydrate growth: implications for carbon storage, Chem. Eng. J. 418 (2021), 129423.
- [25] A. Phan, M. Stamatakis, C.A. Koh, A. Striolo, Wetting properties of clathrate hydrates in the presence of polycyclic aromatic compounds: evidence of ionspecific effects, J. Phys. Chem. Lett. 13 (2022) 8200–8206.
- [26] H.P. Veluswamy, Q.W. Hong, P. Linga, Morphology study of methane hydrate formation and dissociation in the presence of amino acid, Cryst. Growth Des. 16 (2016) 5932–5945.
- [27] H. Kim, H.P. Veluswamy, Y. Seo, P. Linga, Morphology study on the effect of thermodynamic inhibitors during methane hydrate formation in the presence of NaCl, Cryst. Growth Des. 18 (2018) 6984–6994.
- [28] G. Song, Y. Ning, P. Guo, Y. Li, W. Wang, Investigation on hydrate growth at the oil-water interface: in the presence of wax and surfactant, Langmuir 37 (2021) 6838–6845.
- [29] S. Dong, C. Liu, W. Han, M. Li, J. Zhang, G. Chen, The effect of the hydrate antiagglomerant on hydrate crystallization at the oil-water interface, ACS Omega 5 (2020) 3315–3321.
- [30] J.M. Miguez, M.M. Conde, J.P. Torre, F.J. Blas, M.M. Pineiro, C. Vega, Molecular dynamics simulation of CO2 hydrates: prediction of three phase coexistence line, J. Chem. Phys. 142 (2015).
- [31] T. Yagasaki, M. Matsumoto, H. Tanaka, Mechanism of slow crystal growth of tetrahydrofuran clathrate hydrate, J. Phys. Chem. C 120 (2016) 3305–3313.
- [32] P.-W. Wang, D.T. Wu, S.-T. Lin, Promotion mechanism for the growth of CO2 hydrate with urea using molecular dynamics simulations, Chem. Commun. 57 (2021) 5330–5333.
- [33] M.R. Walsh, C.A. Koh, E.D. Sloan, A.K. Sum, D.T. Wu, Microsecond simulations of spontaneous methane hydrate nucleation and growth, Science 326 (2009) 1005, 1009.
- [34] J.M. Schicks, J.A. Ripmeester, The coexistence of two different methane hydrate phases under moderate pressure and temperature conditions: kinetic versus thermodynamic products. Angew. Chem. Int. Ed. 43 (2004) 3310–3313.
- [35] D.K. Staykova, W.F. Kuhs, A.N. Salamatin, T. Hansen, Formation of porous gas hydrates from ice powders: diffraction experiments and multistage model, J. Phys. Chem. B 107 (2003) 10299–10311.
- [36] A. Arjun, P.G. Bolhuis, Homogeneous nucleation of crystalline methane hydrate in molecular dynamics transition paths sampled under realistic conditions, J. Chem. Phys. 158 (2023), 044504.
- [37] M.J. Abraham, T. Murtola, R. Schulz, S. Páll, J.C. Smith, B. Hess, E. Lindahl, GROMACS: high performance molecular simulations through multi-level parallelism from laptops to supercomputers, SoftwareX 1 (2015) 19–25.
- [38] A. Nilsson, F. Perakis, X-ray studies of water, in: E.J. Jaeschke, S. Khan, J. R. Schneider, J.B. Hastings (Eds.), Synchrotron Light Sources and Free-Electron Lasers: Accelerator Physics, Instrumentation and Science Applications, Springer International Publishing, Cham, 2020, pp. 1935–1988.
- [39] M. Lauricella, G. Ciccotti, N.J. English, B. Peters, S. Meloni, Mechanisms and nucleation rate of methane hydrate by dynamical nonequilibrium molecular dynamics, J. Phys. Chem. C 121 (2017) 24223–24234.
- [40] T.A. Berendsen, P.G. Bolhuis, Unbiased atomistic insight in the competing nucleation mechanisms of methane hydrates, Proc. Natl. Acad. Sci. 116 (2019) 19305–19310
- [41] D. Daniel-David, F. Guerton, C. Dicharry, J.-P. Torré, D. Broseta, Hydrate growth at the interface between water and pure or mixed CO2/CH4 gases: Influence of pressure, temperature, gas composition and water-soluble surfactants, Chem. Eng. Sci. 132 (2015) 118–127.
- [42] A. Phan, H.M. Stoner, M. Stamatakis, C.A. Koh, A. Striolo, Surface morphology effects on clathrate hydrate wettability, J. Colloid Interf. Sci. 611 (2022) 421–431.
- [43] H. Fan, D.E. Resasco, A. Striolo, Amphiphilic silica nanoparticles at the decane—water interface: insights from atomistic simulations, Langmuir 27 (2011) 5264–5274.
- [44] A. Khedr, A. Striolo, DPD parameters estimation for simultaneously simulating water-oil interfaces and aqueous nonionic surfactants, J. Chem. Theory Comput. 14 (2018) 6460–6471.
- [45] T. Bui, H. Frampton, S. Huang, I.R. Collins, A. Striolo, A. Michaelides, Water/oil interfacial tension reduction – an interfacial entropy driven process, PCCP 23 (2021) 25075–25085.
- [46] T.T.B. Le, C. Divine-Ayela, A. Striolo, D.R. Cole, Effects of surface contamination on the interfacial properties of CO2/water/calcite systems, PCCP 23 (2021) 1885–18892.
- [47] S. Abbott, Surfactant Science: Principles and Practice (2015).
- [48] J.L.F. Abascal, E. Sanz, R.G. Fernandez, C. Vega, A potential model for the study of ices and amorphous water: TIP4P/Ice, J. Chem. Phys. 122 (2005), 234511.
- [49] M.G. Martin, J.I. Siepmann, Transferable potentials for phase equilibria. 1. Unitedatom description of n-alkanes, J. Phys. Chem. B 102 (1998) 2569–2577.
- [50] J.M. Wang, R.M. Wolf, J.W. Caldwell, P.A. Kollman, D.A. Case, Development and testing of a general amber force field, J. Comput. Chem. 25 (2004) 1157–1174.

- [51] D.A. Case, V. Babin, J.T. Berryman, R.M. Betz, Q. Cai, D.S. Cerutti, T.E.I. Cheatham, T.A. Darden, R.E. Duke, H. Gohlke, A.W. Goetzm, S. Gusarov, N. Homeyer, P. Janowski, J. Kaus, I. Kolossváry, A. Kovalenko, T.S. Lee, S. LeGrand, T.L. Luchko, R., B. Madej, K.M. Merz, F. Paesani, D.R. Roe, A. Roitberg, C. Sagui, R. Salomon-Ferrer, G. Seabra, C.L. Simmerling, W. Smith, J. Swails, R.C. Walker, J. Wang, R.M. Wolf, X. Wu, P.A. Kollman, AMBER 14, University of California, San Francisco. 2014.
- [52] L.X. Dang, Mechanism and thermodynamics of ion selectivity in aqueous-solutions of 18-crown-6 ether - a molecular-dynamics study, J. Am. Chem. Soc. 117 (1995) 6954–6960.
- [53] A. Phan, A. Striolo, Aqueous films on pore surfaces mediate adsorption and transport of gases through crowded nanopores, J. Chem. Phys. 154 (2021), 004706
- [54] J.W. Eastwood, R.W. Hockney, D.N. Lawrence, P3m3dp the 3-dimensional periodic particle-particle-particle-mesh program, Comput. Phys. Commun. 19 (1980) 215–261.
- [55] M.P. Allen, D.J. Tildesley, Computer Simulation of Liquids, Oxford University Press, Oxford, UK, 2004.
- [56] T. Bui, D. Monteiro, L. Vo, A. Striolo, Synergistic and antagonistic effects of aromatics on the agglomeration of gas hydrates, Sci. Rep.-UK 10 (2020) 1–11.
- [57] A. Hassanpouryouzband, J. Yang, B. Tohidi, E. Chuvilin, V. Istomin, B. Bukhanov, A. Cheremisin, Insights into CO2 capture by flue gas hydrate formation: gas composition evolution in systems containing gas hydrates and gas mixtures at stable pressures, ACS Sustain. Chem. Eng. 6 (2018) 5732–5736.
- [58] F. Mahmoudinobar, C.L. Dias, GRADE: A code to determine clathrate hydrate structures, Comput. Phys. Commun. 244 (2019) 385–391.
- [59] E. Dendy Sloan, C.A. Koh, Clathrate Hydrates of Natural Gases, srd ed. ed., CRC Press - Taylor & Francis Group, 2007.
- [60] J.R. Davenport, O.M. Musa, M.J. Paterson, M.-O.-M. Piepenbrock, K. Fucke, J. W. Steed, A simple chemical model for clathrate hydrate inhibition by polyvinylcaprolactam, Chem. Commun. 47 (2011) 9891–9893.
- [61] M. Cha, K. Shin, Y. Seo, J.-Y. Shin, S.-P. Kang, Catastrophic growth of gas hydrates in the presence of kinetic hydrate inhibitors, Chem. A Eur. J. 117 (2013) 13988–13995.
- [62] T. Yagasaki, M. Matsumoto, H. Tanaka, Adsorption of kinetic hydrate inhibitors on growing surfaces: a molecular dynamics study, J. Phys. Chem. B 122 (2018) 3396–3406.
- [63] M.A. Kelland, T.M. Svartaas, J. Øvsthus, T. Tomita, J.-I. Chosa, Studies on some zwitterionic surfactant gas hydrate anti-agglomerants, Chem. Eng. Sci. 61 (2006) 4048–4059.
- [64] M.A. Kelland, T.M. Svartaas, J. Øvsthus, T. Tomita, K. Mizuta, Studies on some alkylamide surfactant gas hydrate anti-agglomerants, Chem. Eng. Sci. 61 (2006) 4290–4298.
- [65] D. Jin, B. Coasne, Molecular simulation of the phase diagram of methane hydrate: free energy calculations, direct coexistence method, and hyperparallel tempering, Langmuir 33 (2017) 11217–11230.
- [66] M. Ohtake, Y. Yamamoto, T. Kawamura, A. Wakisaka, W.F. de Souza, A.M.V. de Freitas, Clustering structure of aqueous solution of kinetic inhibitor of gas hydrates, J. Phys. Chem. B 109 (2005) 16879–16885.
- [67] S.K. Prasad, J.S. Sangwai, Impact of lighter alkanes on the formation and dissociation kinetics of methane hydrate in oil-in-water dispersions relevant for flow assurance, Fuel 333 (2023), 126500.
- [68] Y. Zhong, R.E. Rogers, Surfactant effects on gas hydrate formation, Chem. Eng. Sci. 55 (2000) 4175–4187.
- [69] Z.-G. Sun, R.-S. Ma, R.-Z. Wang, K.-H. Guo, S.-S. Fa, Experimental studying of additives effects on gas storage in hydrates, Energ. Fuel 17 (2003) 1180–1185.
- [70] K. Watanabe, S. Imai, Y.H. Mori, Surfactant effects on hydrate formation in an unstirred gas/liquid system: an experimental study using HFC-32 and sodium dodecyl sulfate, Chem. Eng. Sci. 60 (2005) 4846–4857.
- [71] P. Di Profio, S. Arca, R. Germani, G. Savelli, Surfactant promoting effects on clathrate hydrate formation: are micelles really involved? Chem. Eng. Sci. 60 (2005) 4141–4145.
- [72] J. Yoslim, P. Linga, P. Englezos, Enhanced growth of methane–propane clathrate hydrate crystals with sodium dodecyl sulfate, sodium tetradecyl sulfate, and sodium hexadecyl sulfate surfactants, J. Cryst. Growth 313 (2010) 68–80.
- [73] Z.-Y. Lin, D.T. Wu, S.-T. Lin, Equilibrium and transport properties of methane at the methane/water interface with the presence of SDS, J. Phys. Chem. C 122 (2018) 29259–29267.
- [74] C.-Y. Sun, G.-J. Chen, L.-Y. Yang, Interfacial tension of methane + water with surfactant near the hydrate formation conditions, J. Chem. Eng. Data 49 (2004) 1023–1025.
- [75] A.P. Willard, D. Chandler, Instantaneous liquid interfaces, J. Phys. Chem. B 114 (2010) 1954–1958.
- [76] J.S. Hub, B.L. de Groot, D. van der Spoel, g wham-a free weighted histogram analysis implementation including robust error and autocorrelation estimates, J. Chem. Theory Comput. 6 (2010) 3713–3720.
- [77] S.K. Reed, R.E. Westacott, The interface between water and a hydrophobic gas, PCCP 10 (2008) 4614–4622.
- [78] H.S. Ashbaugh, B.A. Pethica, Alkane adsorption at the water—vapor interface, Langmuir 19 (2003) 7638–7645.
- [79] J. Kim, Y. Tian, J. Wu, Thermodynamic and structural evidence for reduced hydrogen bonding among water molecules near small hydrophobic solutes, J. Phys. Chem. B 119 (2015) 12108–12116.
- [80] N.N. Nguyen, A.V. Nguyen, L.X. Dang, The inhibition of methane hydrate formation by water alignment underneath surface adsorption of surfactants, Fuel 197 (2017) 488–496.

- [81] S. Hosseinpour, V. Götz, W. Peukert, Effect of surfactants on the molecular structure of the buried oil/water interface, Angew. Chem. Int. Ed. 60 (2021) 25143–25150.
- [82] N. Ansari, T. Karmakar, M. Parrinello, Molecular mechanism of gas solubility in liquid: constant chemical potential molecular dynamics simulations, J. Chem. Theory Comput. 16 (2020) 5279–5286.
- [83] M. Sega, G. Hantal, B. Fábián, P. Jedlovszky, Pytim: a python package for the interfacial analysis of molecular simulations, J. Comput. Chem. 39 (2018) 2118–2125.
- [84] N. Kumar, M.J. Servis, Z. Liu, A.E. Clark, Competitive interactions at electrolyte/ octanol interfaces: a molecular perspective, J. Phys. Chem. C 124 (2020) 10924–10934.
- [85] V. Venkateshwaran, S. Vembanur, S. Garde, Water-mediated ion-ion interactions are enhanced at the water vapor-liquid interface, Proc. Natl. Acad. Sci. 111 (2014) 8729-8734.